Available online at www.sciencedirect.com

ScienceDirect

Ceramics International 39 (2013) 9343–9349

CERAMICS INTERNATIONAL

www.elsevier.com/locate/ceramint

Characterization and photoluminescent properties of sol–gel-derived $Ca_{2(1-x)}La_{7.6+x}(SiO_4)_6O_2$:$Eu_{0.4}$, Li_x phosphors

Naixu Li, Bingyao Zhou, Shuqiang Li, Jiancheng Zhou*, Yueming Sun

School of Chemistry and Chemical Engineering, Southeast University, Nanjing, Jiangsu 211189, People's Republic of China

Received 10 April 2013; received in revised form 7 May 2013; accepted 13 May 2013
Available online 22 May 2013

Abstract

Red-emitting $Ca_{2(1-x)}La_{7.6+x}(SiO_4)_6O_2$:$Eu_{0.4}$, Li_x (CLS:$Eu_{0.4}$, Li_x) phosphors were synthesized via a citric acid based sol–gel combustion method. The morphologies, crystal structures and optical properties of these phosphors were characterized by scanning electron microscopy (SEM) and transmission electron microscopy (TEM), powder X-ray diffraction (PXRD) and photoluminescence (PL) spectroscopy, respectively. The CLS:$Eu_{0.4}$ based phosphors readily excited under UV light (387 nm), which makes them promising red-emitting candidates for commercial near-UV light emitting diodes (LEDs)-pumped white LEDs. After doping with Li^+ ions, the CLS:$Eu_{0.4}$, Li_x phosphors exhibited remarkably enhanced photoluminescent performances. Additionally, the emission intensity of CLS:$Eu_{0.4}$, Li_x phosphors generated using the sol–gel combustion method was found to be much higher than for those obtained using a solid-state reaction method. This finding indicated the sol–gel combustion method could be considered a versatile route for producing high-quality CLS:$Eu_{0.4}$, Li_x phosphors.

Keywords: C. Optical properties; Sol–gel combustion; Red-emitting phosphor

1. Introduction

Solid-state lighting (SSL) for white-light generation has attracted enormous interest since the advent of light emitting diodes (LEDs) because it offers long lifetimes, high energy efficiencies, and positive environment effects relative to incandescent and fluorescent lamps [1,2]. To generate white light, LEDs are typically integrated with phosphors that convert the intrinsic blue light to other colors [3]. A common phosphor is yttrium aluminum garnet (YAG) doped with Ce^{3+} ions [4]. However, such integrations are plagued by their low correlated color temperatures (CCTs), which limit their color rendering indexes (CRIs). Typically, white light can only be produced with a CCT from 4000 to 8000 K, which corresponds to the neutral to cool-white interval. The CRIs for such LEDs is typically below 80 due to the absence of a red component in the generated light [2]. To overcome these disadvantages, red-emitting phosphors, such as sulfide phosphors (e.g., $(Ca_{1-x}, Sr_x)S:Eu^{2+}$ and $Y_2O_2S:Eu^{3+}$), are also included [5–8]. However, these compounds exhibit poor chemical stability at high temperatures and are thus limited in their application. In a sense, producing LEDs containing luminescent materials with robust chemical stabilities remains a significant technical challenge for creating white-light generators with reasonably satisfactory performances.

Recently, silicates with oxyapatite-type structure have been studied widely as promising red-emitting phosphors [9–14]. This interest stems from the improved chemical stability gained from the presence of SiO_4 units. The general formula for an oxyapatite-type silicate compound is $A_4B_6(SiO_4)_6O_2$. This type of compound crystallizes as a hexagonal system with the space group $P6_3/m$ [15]. A (4*f*) and B (6*h*) are two distinct crystallographic sites that can both accommodate alkali, alkaline-earth, or rare-earth metal atoms. The A site has trigonal point symmetry (C_3) due to the tricapped trigonal prism formed by the nine oxygen atoms surrounding the cationic site. In contrast, the B site has a sevenfold coordination with a local symmetry of C_s, which involves six oxygen atoms and one O^{2-} anion. Such a unique crystal structure allows for the convenient accommodation of various combinations of metal ions into the A and B sites [16,17].

Thanks to the research efforts of many groups, it is now possible to fabricate oxyapatite-type silicates that incorporate a

*Corresponding author. Tel.: +86 13 914766900.
E-mail address: jczhou@seu.edu.cn (J. Zhou).

0272-8842/$ - see front matter © 2013 Elsevier Ltd and Techna Group S.r.l. All rights reserved.
http://dx.doi.org/10.1016/j.ceramint.2013.05.051

myriad of metals ions. For example, Boyer and co-workers synthesized and characterized the luminescent properties of Eu^{3+}-doped $Ca_xLa_{10-x}(SiO_4)_y(PO_4)_{6-y}$ [10]. Leu and co-workers reported the synthesis of oxyapatite-type $(Sr_2RE_2)(RE_6)(SiO_4)_6O_2$ (RE = La, Pr, Tb, Tm, and Y) compounds using conventional solid-state methods [15]. Dong and co-workers studied and described cation distributions in Eu^{3+}-doped $Sr_2Y_8(SiO_4)_6O_2$ phosphors [18]. These successful demonstrations not only enable the versatile syntheses of oxyapatite-type silicates but also enrich our understanding of the luminescent properties of such compounds.

As indicated in Dong's study, the B (6*h*) sites are fully occupied by lanthanide (i.e., Y^{3+}) ions while the A (4*f*) sites are filled with a random combination of lanthanide ions and bivalent cations (i.e., Ca^{2+}) [19]. Replacing a bivalent ion in the A sites with a second type of trivalent lanthanide ion may generate holes or oxygen defects due to their different valent states. The presence of such holes or oxygen defects in the compound could significantly quench radiative energy transitions and change the symmetry of the A site. Both of these consequences could negatively influence the luminescent performances of the compound. Incorporating an appropriate amount of monovalent (i.e., Li^+) ions may help eliminate such holes or defects. However, given the different atomic radii of monovalent and bivalent ions, underestimating the possible effects of incorporating monovalent ions remains risky because the lattice parameters and local symmetry of the crystal structure may change. Therefore, a systematic study is highly desirable. In addition, most previous studies used conventional solid-state methodologies, which require high reaction temperatures and long reaction times to obtain well-crystallized and phase-pure phosphors. In contrast, the sol–gel method can substantially reduce the heating temperature and reaction time due to the high homogeneity of the precursors, which saves energy during phosphor preparation.

Herein, we present a systematic study of the synthetic and photoluminescent properties of oxyapatite-type silicates, $Ca_{2(1-x)}La_{7.6+x}(SiO_4)_6O_2$ (CLS), co-doped with trivalent (Eu^{3+}) and monovalent (Li^+) ions. A series of pure-phase silicate oxyapatite materials, including CLS:$Eu_{0.4}$, and CLS:$Eu_{0.4}$, Li_x, were synthesized using a citric acid based sol–gel combustion method. The crystal structures and photoluminescent properties of these compounds were characterized by powder X-ray diffraction (PXRD) and photoluminescence (PL) spectroscopy, respectively. The effect of the Li^+ ion concentration on the crystal structure and luminescent properties of the CLS:$Eu_{0.4}$, Li_x material were investigated. In addition, we compared the PL performance of CLS:$Eu_{0.4}$, Li_x phosphors generated via two methods: sol–gel combustion and conventional solid-state reaction.

2. Experimental procedure

2.1. Synthesis of $Ca_{2(1-x)}La_{7.6+x}(SiO_4)_6O_2$:$Eu_{0.4}$, Li_x phosphors

Analytical reagent grade of calcium nitrate ($Ca(NO_3)_2 \cdot 4H_2O$), lanthanum nitrate ($La(NO_3)_3 \cdot 6H_2O$), europium nitrate ($Eu(NO_3)_3 \cdot 6H_2O$), lithium nitrate ($LiNO_3$), citric acid ($C_6H_8O_7 \cdot H_2O$), tetraethyl orthosilicate ($(C_2H_5)_4SiO_4$), and ethanol (C_2H_5OH) were obtained from Shanghai Chemicals Company and used without purification. All aqueous solutions were prepared using deionized water with a resistivity of 18.2 MΩ cm. In a standard synthesis of $Ca_{2(1-x)}La_{7.6+x}(SiO_4)_6O_2$:$Eu_{0.4}$, Li_x (CLS:$Eu_{0.4}$, Li_x) via the sol–gel combustion method, La^{3+}, Ca^{2+}, Li^+, and Eu^{3+} nitrates are mixed in stoichiometric amounts with citric acid in deionized water in a 100 mL beaker. The molar ratio of the total metal cations to citric acid was 1:3. After the mixture became clear, an ethanol solution containing stoichiometric amounts of $(C_2H_5)_4SiO_4$ was slowly added with continuous magnetic stirring and heating at 80 °C. As the water evaporated, the solution gradually became viscous, and a transparent gel finally formed. This gel was dried in a vacuum oven at 120 °C for 24 h before sintering in a furnace maintained at a certain temperature (i.e., 800 °C, 900 °C, 1000 °C, 1100 °C, and 1200 °C) for 3 h. To generate the CLS:$Eu_{0.4}$, $Li_{0.03}$ phosphor via a solid-state reaction, A.R. grade SiO_2, La_2O_3, $CaCO_3$, Li_2CO_3 and Eu_2O_3 were thoroughly mixed in stoichiometric amounts and ground in an agate mortar with ethanol to obtain a homogeneous chemical mixture. The mixture was dried in an oven set to 80 °C for 3 h. Finally, the dried powder mixture was transferred to a corundum crucible and sintered in an oven set to 1400 °C for 5 h.

2.2. Characterizations

Powder X-ray diffraction patterns were collected using an X'Pert Pro X-ray diffractometer (PANalytical B.V.) with a Cu K_α rotating anode source and generator settings of 40 kV and 40 mA. The samples were measured in the 2θ range from 10° to 70° with a step size of 0.02 and scan speed of 2 °/min. The size and shape of the samples were analyzed using a scanning electron microscope (JSM-5600LV, JEOL) and transmission electron microscope (H-7500, Hitachi). The excitation and emission spectra were measured at room temperature using a FluoroMax-4 fluorescence spectrophotometer (HORIBA Jobin Yvon).

3. Results and discussion

3.1. Crystal structure and characterization

The sintering temperature is generally accepted to be a critical parameter for the sol–gel combustion method. Thus, we conducted a set of experiments to determine the best sintering temperature for forming CLS:$Eu_{0.4}$ compounds with high purity. Fig. 1a shows the PXRD patterns for powdered CLS:$Eu_{0.4}$ samples obtained using different sintering temperatures ranging from 800 to 1200 °C. A reference CLS pattern with a hexagonal crystal structure (JCPDS, file no. 29-337) is also shown in Fig. 1a for comparison [20]. The CLS:$Eu_{0.4}$ samples sintered at 1100 and 1200 °C both largely indexed to the reference CLS pattern. For samples sintered at a lower temperature (800, 900 and 1000 °C), some impurities were detected in the PXRD patterns, including La_2CaO_x (JCPDS, file no. 42-342), hexagonal La_2O_3 (JCPDS, file no. 2-688), and hexagonal SiO_2 (JCPDS, file no. 11-252). As a result, we

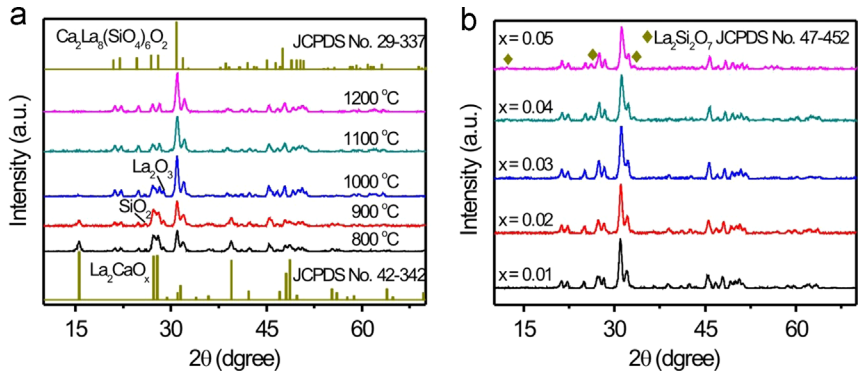

Fig. 1. (a) PXRD patterns for powder CLS:$Eu_{0.4}$ samples obtained at sintering temperatures from 800 to 1200 °C; (b) PXRD patterns for CLS:$Eu_{0.4}$, Li_x powders formed under different Li^+ ion dopings.

believed a sintering temperature of 1100 °C to be the optimized condition for forming CLS-based products with good crystallinity and minimal impurities using the current synthesis.

We further extend this synthetic method to generate CLS materials co-doped with both Eu^{3+} and Li^+ ions. Similar preparations were conducted using the optimized sintering temperature of 1100 °C for all steps except the Li^+ ion doping. The crystal structures of the produced materials were characterized using PXRD. Fig. 1b shows a serious of PXRD patterns for the CLS:$Eu_{0.4}$, Li_x powders formed using different Li^+ ion doping concentrations. The diffraction peaks can be readily indexed to hexagonal CLS, and no impurities were detected for Li^+ ion concentrations of 0.01, 0.02, and 0.03. Higher Li^+ ion concentrations, i.e., $x=0.04$ and 0.05, formed an impurity phase, $La_2Si_2O_7$ (JCPDS, file no. 47-452), in the product. In general, the formation of $La_2Si_2O_7$ via a solid-state synthesis using La_2O_3 and SiO_2 as the starting materials required sintering temperatures as high as 1500 °C [21]. However, in our case, the sintering temperature was only 1100 °C. This result shows that the doped Li^+ ions facilitate the formation of the $La_2Si_2O_7$ phase at lower temperatures, possibly because of the lower melting point of alkali silicate than SiO_2 (Li-silicate, 1200 °C, versus SiO_2, 1600 °C) [22–24]. The XRD-deduced lattice constants of the CLS phase in the CLS:$Eu_{0.4}$, Li_x phosphors are listed in Table 1, where both a and c decrease as the Li^+ doping concentration increases. This decrease in the lattice constants can be ascribed to the substitution of Ca^{2+} by Li^+ and Eu^{3+} because the ionic sizes of Li^+ (0.6 Å) and Eu^{3+} (0.95 Å) are relatively smaller in comparison to Ca^{2+} (0.99 Å).

Table 1
Lattice constants a and c for the $Ca_{2(1-x)}La_{7.6+x}(SiO_4)_6O_2$:$Eu_{0.4}$, Li_x powder samples with different Li^+ doping concentration x.

x	a (Å)	c (Å)
0	9.628	7.103
0.01	9.624	7.074
0.02	9.604	7.052
0.03	9.597	7.045
0.04	9.587	7.036
0.05	9.492	7.022

3.2. Photoluminescence properties

Fig. 2 shows the excitation and emission spectra for both the CLS:$Eu_{0.4}$ and CLS:$Eu_{0.4}$, $Li_{0.01}$ phosphors obtained using a sintering temperature of 1100 °C. These spectra were recorded using an emission wavelength of 611 nm and excitation wavelength of 387 nm. The peaks in the emission spectra of both phosphors were primarily located in the wavelength range of 550–720 nm. These peaks correspond to the transitions from the $^5D_0$ state to the ^7F_j ($j=0$, 1, 2, 3 or 4) state for the $4f^6$ configuration of Eu^{3+} ions. Emissions were not detected from higher excitation levels, such as $^5D_1$, which indicates an efficient non-radiative relaxation to the $^5D_0$ level occurred. The electric-dipole (ED) transition of the Eu^{3+} ions ($^5D_0 \rightarrow {}^7F_2$) creates a set of red emissions in the range from 600 to 625 nm. The emissions from the Eu^{3+} ions centered at 590 nm could be identified as the parity-allowed magnetic dipole (MD) transition from $^5D_0 \rightarrow {}^7F_1$ [25–27]. The peak corresponding to the $^5D_0 \rightarrow {}^7F_2$ transition was the most intense, as marked in Fig. 2a. We note that the peak corresponding to the $^5D_0 \rightarrow {}^7F_0$ transition was observed in the spectra. However, the $^5D_0 \rightarrow {}^7F_0$ transition ($J=0 \rightarrow J=0$) is parity-forbidden according to the selection rules of the Judd–Ofelt theory [28]. The abnormal appearance of the $^5D_0 \rightarrow {}^7F_0$ transition could be due to the strong linear crystal field component present at the Eu^{3+} site. This forbidden transition increases in intensity after J–J mixing [29]. In addition, we noticed several sharp excitation bands that are characteristic of the f–f transitions of Eu^{3+} ions in the $4f^6$ configuration, and the sharp f–f transitions of Eu^{3+} ($^7F_0 \rightarrow {}^5D_{1,2,3,4}$, $^5L_{6,7}$) are clearly marked in Fig. 2b. Of these excitation transitions, $^7F_0 \rightarrow {}^5L_6$ (387 nm) provides a relatively intense peak [30] that matches those of commercially available near-UV LED chips [31,32].

Oxyapatite-type silicate materials belong to a large family of isomorphous compounds in the space group $P6_3/m$ with an empirical formula of $A_4B_6(SiO_4)_6O_2$. This structure contains two cationic sites labeled A and B. For $Ca_2La_8(SiO_4)_6O_2$, the B sites are fully occupied by La^{3+} ions, while the A sites are

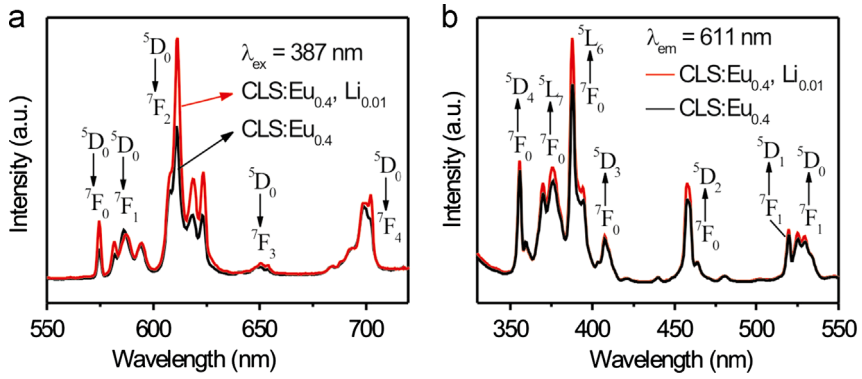

Fig. 2. (a) Emission and (b) excitation spectra for both CLS:$Eu_{0.4}$ and CLS:$Eu_{0.4}$, $Li_{0.01}$ phosphors obtained at a sintering temperature of 1100 °C.

occupied by a random distribution of both Ca^{2+} and La^{3+} ions [33]. As shown in Fig. 3, the Ca^{2+} and La^{3+} ions share the A sites and form polyhedra with a local symmetry of C_3. The nine coordinated oxygen ions, including three O1, three O2 and three O3, form a tricapped trigonal-prismatic geometry (Fig. 3b). The B site is located in a sevenfold coordination polyhedra with a local symmetry of C_s and seven oxygen atoms (one O1, one O2, four O3, and one O4) which form an irregular polyhedra with pentagonal bipyramidal geometry, as shown in Fig. 3c. Generally, the ^7F_J energy levels of the Eu^{3+} will split due to the crystal field effects of the surrounding ions [34]. For the B site, the number of split components for the allowed $^5D_0 \rightarrow {}^7F_1$ and $^5D_0 \rightarrow {}^7F_2$ transitions for the C_s symmetry group are 3 and 5, respectively, according to the completely lifted "2J+1" degeneracy. In contrast, the slightly higher C_3 symmetry for A provide 2 and 3 split components for the $^5D_0 \rightarrow {}^7F_1$ and $^5D_0 \rightarrow {}^7F_2$ transitions, respectively [35,36]. However, we only found 3 and 4 Stark components for the $^5D_0 \rightarrow {}^7F_1$ and $^5D_0 \rightarrow {}^7F_2$ transitions, respectively, in the emission spectra shown in Fig. 2a because the Eu^{3+} ions are distributed in both the A and B sites, which may result in the superposition of emission peaks from different sites.

In addition, we noticed that the intensities of the emission peaks caused by both the $^5D_0 \rightarrow {}^7F_1$ and $^5D_0 \rightarrow {}^7F_4$ transitions were abnormally high. This phenomenon usually occurred when the Eu^{3+} ions were located in the inversion center [37]. However, in an oxyapatite structure, there is no inversion center [38]. Therefore, the local geometries of the occupied Eu^{3+} ion sites have distorted to form an inversion center in the current product. Typically, if a divalent metallic cation, such as Ca^{2+}, is replaced by a trivalent metallic cation, Eu^{3+}, the host must absorb O_2 from the air to maintain charge balance. These O_2 molecules in the host would generate oxygen defects and thus change the geometry of the Eu^{3+} ion sites [39]. In this case, it is possible that the location of the Eu^{3+} ions became an inversion center, which enhanced the emissions from both the $^5D_0 \rightarrow {}^7F_1$ and $^5D_0 \rightarrow {}^7F_4$ transitions.

In addition, two differences in the emission and excitation spectra shown in Fig. 2 after doping the CLS:$Eu_{0.4}$ phosphor with the Li^+ ions should be noted: (i) the emission intensity of the $^5D_0 \rightarrow {}^7F_2$ transition increased by an enhancement factor of 1.56; (ii) the I_{0-2}/I_{0-1} ratio varied from 3.16 to 4.68. Based on these results, it is not unreasonable to assume that the Li^+ ion

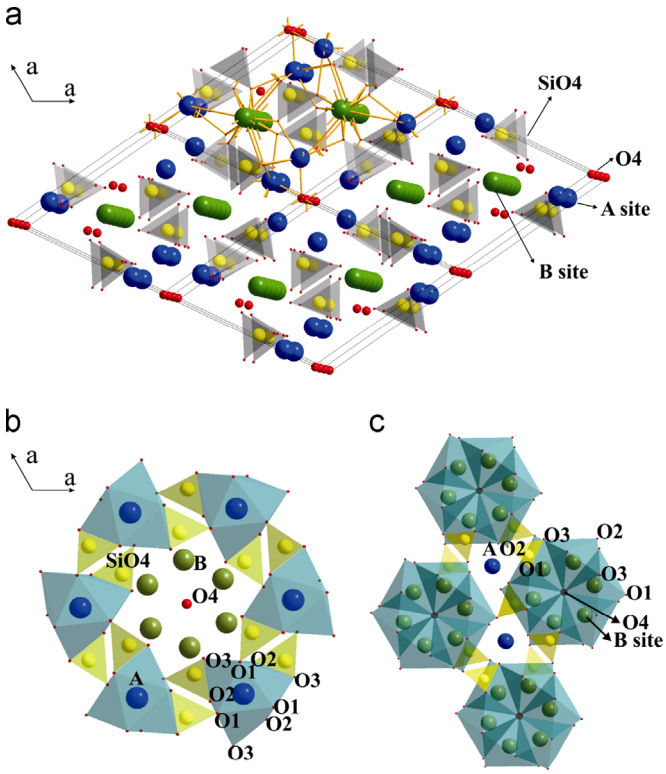

Fig. 3. (a) The crystal structure of $Ca_2La_8(SiO_4)_6O_2$; the blue, green, yellow and red spheres represent the A site, the B site, silicon and oxygen atoms, respectively; (b) A–O polyhedra and (c) B–O polyhedra and the Si–O tetrahedra configurations along the c-axis. (For interpretation of the references to color in this figure legend, the reader is referred to the web version of this article.)

doping could benefit the PL performance of the CLS:$Eu_{0.4}$ phosphors. There are two factors that may be responsible for such an improvement. On the one hand, incorporating Li^+ into the CLS host can eliminate oxygen defects that arise from charge compensation and thus effectively prevent the radiative transitions from being quenched. On the other hand, the absence of these oxygen defects in the phosphor also eliminates the inversion center [40]. In this case, emissions from the $^5D_0 \rightarrow {}^7F_2$ transition become dominant, while the undesired emissions, such as $^5D_0 \rightarrow {}^7F_1$ and $^5D_0 \rightarrow {}^7F_4$, were dampened. In other words, most of the energy would be consumed by the desired radiative transitions and thus contribute to enhancing the red-emission efficiency.

To further elucidate the effect that Li^+ ions have on the PL performance of the product, we attempted to manipulate the Li^+ ion concentration in the phosphor. Fig. 4 shows the emission spectra of CLS:$Eu_{0.4}$, Li_x as a function of the Li^+ ion concentration using an excitation wavelength of 387 nm. The emission intensities for the $^5D_0 \rightarrow {}^7F_1$, $^5D_0 \rightarrow {}^7F_2$ and $^5D_0 \rightarrow {}^7F_4$ transitions are summarized in Fig. 5a. It is worth noting that the emission intensity for the $^5D_0 \rightarrow {}^7F_2$ transition increased by an enhancement factor of 2.25 as the Li^+ ion concentration increased from 0 to 0.03. The other emissions followed similar trends as the Li^+ ions increased in concentration. Interestingly, the intensity decreased when the Li^+ ion concentration was above 0.03. This phenomenon might be attributed to the following two factors: (i) As shown in Table 1, the crystallographic lattice constants decreased as the Li^+ doping concentration increases. A shorter Eu^{3+}–Eu^{3+} distance would enhance energy transfer between the Eu^{3+} ions [41]; (ii) a higher Li^+ ion concentration can promote the formation of impurities, such as $La_2Si_2O_7$, that may weaken the emission. In short, to achieve the best red-emitting phosphor performance, the Li^+ ion concentration should be set within an appropriate range for the current synthesis. We also summarize the variations in the intensity ratios for the CLS:$Eu_{0.4}$, Li_x phosphors (I_{0-2}/I_{0-1}, I_{0-2}/I_{0-4}) with an excitation wavelength of 387 nm. As shown in Fig. 5b, the intensity ratios for I_{0-2}/I_{0-1} and I_{0-2}/I_{0-4} increased with the concentration of the Li^+ ions and reached a maximum, i.e., 5.71 and 3.25, respectively, at $x=0.03$ because the defect regions in the phosphor had largely been removed. Even higher Li^+ ion concentrations no longer favored the increased I_{0-2}/I_{0-1} and I_{0-2}/I_{0-4} ratios. The aforementioned shortened Eu^{3+}–Eu^{3+} distance and the presence of $La_2Si_2O_7$ should be responsible for this variation.

We also compared the PL properties of CLS:$Eu_{0.4}$, $Li_{0.03}$ phosphors prepared via the sol–gel and solid state reaction methods. Fig. 6 shows the emission spectra for the two CLS:$Eu_{0.4}$, $Li_{0.03}$ phosphors. Both phosphors exhibited similar emission behaviors, which indicate they had similar crystal structures. However, it is worth noting that the emission intensities of those phosphors prepared via the sol–gel combustion method were much higher than for those prepared via the solid-state reaction method. Fig. 7 shows the SEM and TEM images of the CLS:$Eu_{0.4}$, $Li_{0.03}$ phosphors prepared via the sol–gel and solid state reaction methods. The size of the obtained sol–gel samples was approximately 300 nm. The size of the sample prepared via the solid state reaction route was approximately 500 nm. Moreover, as indicated in the insets, the particles prepared via the solid state method were covered with many small particles, which created a much coarser surface than for those prepared via the sol–gel method.

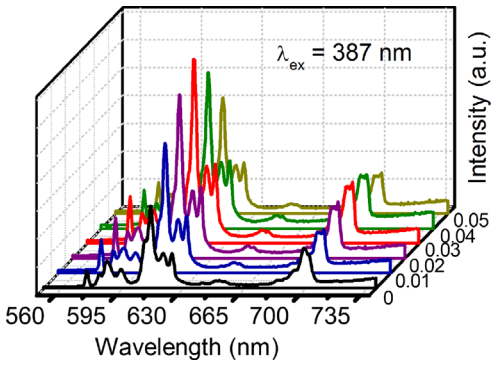

Fig. 4. Emission spectra for CLS:$Eu_{0.4}$, Li_x as a function of the Li^+ ion concentration with an excitation wavelength of 387 nm.

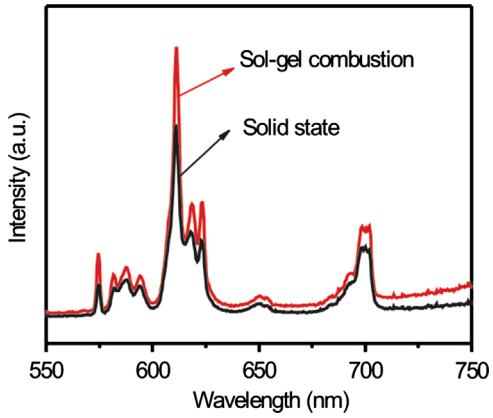

Fig. 6. Emission spectra for two CLS:$Eu_{0.4}$, $Li_{0.03}$ phosphors prepared by either the sol–gel method or the solid state reaction methods.

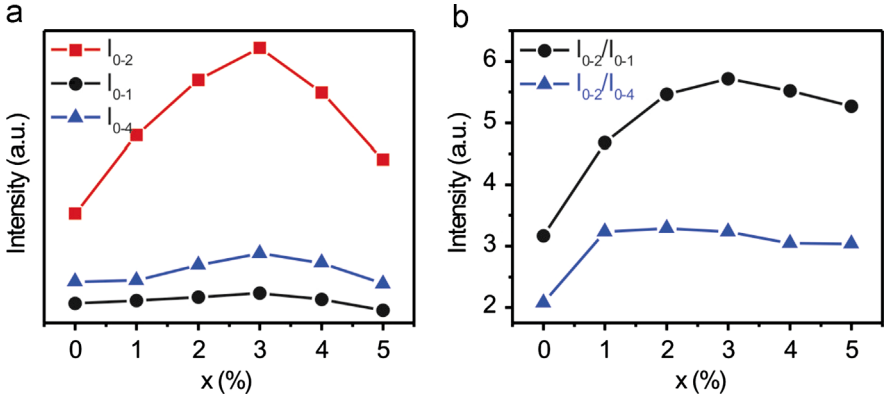

Fig. 5. (a) Emission intensity for $^5D_0 \rightarrow {}^7F_1$, $^5D_0 \rightarrow {}^7F_2$ and $^5D_0 \rightarrow {}^7F_4$ (i.e., I_{0-1}, I_{0-2} and I_{0-4}) transitions as a function of the Li^+ ion concentration and (b) intensity ratios of CLS:$Eu_{0.4}$, Li_x phosphors (I_{0-2}/I_{0-1}, I_{0-2}/I_{0-4}) with an excitation wavelength of 387 nm.

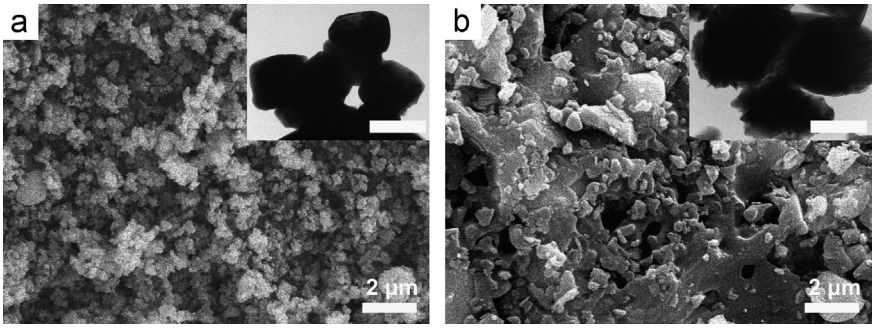

Fig. 7. SEM images of the two CLS:$Eu_{0.4}$, $Li_{0.03}$ phosphors prepared by the (a) sol–gel method and (b) solid state reaction methods. Insets are the corresponding TEM images. The scale bars in the insets are 300 nm.

Compared to the solid-state reaction, the sol–gel method possesses the significant advantage of atomic-level mixing uniformity for the starting ingredients (e.g., host material and doping element) to generate products with homogeneously distributed metal ions and fewer surface defects. These advantages may account for the higher emission intensity.

4. Conclusions

In summary, we successfully synthesized red-emitting $Ca_{2(1-x)}La_{7.6+x}(SiO_4)_6O_2$:$Eu_{0.4}$, Li_x (CLS:$Eu_{0.4}$, Li_x) phosphors using a citric acid based sol–gel combustion method. The crystal structures of these phosphors were confirmed by powder X-ray diffraction (PXRD). A sintering temperature of 1100 °C favored the formation of CLS:$Eu_{0.4}$ and CLS:$Eu_{0.4}$, Li_x products with high purities. Photoluminescent studies showed that the CLS:$Eu_{0.4}$ based phosphors could be readily excited by near-UV (387 nm) irradiation, which makes them promising red-emitting candidates for commercial near-UV LED-pumped white LEDs. After doping with Li^+ ions, the CLS:$Eu_{0.4}$, Li_x phosphors exhibited remarkably enhanced photoluminescent performances. In addition, the emission intensity of the $^5D_0 \rightarrow {}^7F_2$ transition increased by an enhancement factor of 2.25, and the I_{0-2}/I_{0-1} ratios varied from 3.16 to 5.71. Two possible factors could be responsible for such improvements: (i) the incorporation of Li^+ into the CLS host could eliminate oxygen defects from charge compensation and thus prevent the radiative transitions from being quenched, and (ii) the absence of oxygen defects in these phosphors would also eliminate the inversion center and dampen undesired transitions. Additionally, the emission intensities of the CLS:$Eu_{0.4}$, Li_x phosphors generated via the sol–gel combustion method were much higher than for those obtained via the solid-state reaction method.

Acknowledgment

This work was financially supported by the National Nature Science Foundation of China (No. 31070517) and the National Basic Research Program of China (973 Program, No. 2013CB932902).

References

[1] S. Pimputkar, J.S. Speck, S.P. DenBaars, S. Nakamura, Prospects for LED lighting, Nature Photonics 3 (2009) 180–182.
[2] E.F. Schubert, J.K. Kim, Solid-state light sources getting smart, Science 308 (2005) 1274–1278.
[3] J.S. Kim, P.E. Jeon, Y.H. Park, J.C. Choi, H.L. Park, G.C. Kim, T.W. Kim, White-light generation through ultraviolet-emitting diode and white-emitting phosphor, Applied Physics Letters 85 (2004) 3696–3698.
[4] Y.C. Kang, I.W. Lenggoro, S.B. Park, K. Okuyama, YAG:Ce phosphor particles prepared by ultrasonic spray pyrolysis, Materials Research Bulletin 35 (2000) 789–798.
[5] H. Nanto, Y. Douguchi, J.I. Nishishita, M. Kadota, N. Kashiwagi, T. Shinkawa, S. Nasu, Novel erasable and rewritable optical memory utilizing photostimulated luminescence in Eu and Sm codoped SrS phosphor ceramics, Japanese Journal of Applied Physics 36 (1997) 421–423.
[6] Y. Hu, W. Zhuang, H. Ye, S. Zhang, Y. Fang, X. Huang, Preparation and luminescent properties of (Ca_{1-x}, Sr_x)S: Eu^{2+} red-emitting phosphor for white LED, Journal of Luminescence 111 (2005) 139–145.
[7] K. Swiatek, M. Godlewski, L. Niinisto, M. Leskela, Optical recombination mechanisms in Eu^{2+}-doped CaS and SrS thin films, Journal of Applied Physics 74 (1993) 3442–3446.
[8] L.D. da Vila, E.B. Stucchi, M.R. Davolos, Preparation and characterization of uniform, spherical particles of Y_2O_2S and Y_2O_2S:Eu, Journal of Materials Chemistry 7 (1997) 2113–2116.
[9] A. Yamane, T. Kunimoto, K. Ohmi, T. Honma, H. Kobayashi, Luminescent properties of Tb-activated rare-earth oxyapatite silicate $MLn_4Si_3O_{13}$ (M=Ca, Sr, Ln=La, Gd), Physica Status Solidi C 3 (2006) 2705–2708.
[10] L. Boyer, B. Piriou, J. Carpena, J.L. Lacout, Study of sites occupation and chemical environment of Eu_{3+} in phosphate-silicates oxyapatites by luminescence, Journal of Alloys and Compounds 311 (2000) 143–152.
[11] Z. Dong, Y. Shen, Photoluminescence properties and tem characterization of europium doped silicate oxyapatite $Sr_2Y_8(SiO_4)_6O_2$, Microscopy and Microanalysis 18 (2012) 1904–1905.
[12] C. Peng, G. Li, Z. Hou, M. Shang, J. Lin, Electrospinning synthesis and luminescent properties of one-dimensional $Ca_2Gd_8(SiO_4)_6O_2:Eu^{3+}$ microfibers and microbelts, Materials Chemistry and Physics 136 (2012) 1008–1014.
[13] X. Wang, J. Gan, Y. Huang, H.J. Seo, The doping concentration dependent tunable yellow luminescence of $Sr_5(PO_4)_2(SiO_4):Eu^{2+}$, Ceramics International 38 (2012) 701–706.
[14] Y. Wen, Y. Wang, B. Liu, F. Zhang, Luminescence properties of $Ca_4Y_6(SiO_4)_6O:RE^{3+}$ (RE=Eu, Tb, Dy, Sm and Tm) under vacuum ultraviolet excitation, Optical Materials 34 (2012) 889–892.
[15] L.C. Leu, S. Thomas, M.T. Sebastian, S. Zdzieszynski, S. Misture, R. Ubic, Crystal structure of apatite type rare-earth silicate $(Sr_2RE_2)(RE_6)(SiO_4)_6O_2$ (RE=La, Pr, Tb, Tm, and Y), Journal of the American Ceramic Society 94 (2011) 2625–2632.

[16] G.S.R. Raju, Y.H. Ko, E. Pavitra, J.S. Yu, J.Y. Park, H.C. Jung, B.K. Moon, Formation of $Ca_2Gd_8(SiO_4)_6O_2$ nanorod bundles based on crystal splitting by mixed solvothermal and hydrothermal reaction methods, Crystal Growth and Design 12 (2011) 960–969.
[17] R. El Ouenzerfi, G. Panczer, C. Goutaudier, M.T. Cohen-Adad, G. Boulon, M. Trabelsi-Ayedi, N. Kbir-Ariguib, Relationships between structural and luminescence properties in Eu^{3+}-doped oxyphosphate-silicate apatite $Ca_{2+x}La_{8-x}(SiO4)_{6-x}(PO_4)_xO_2$, Optical Materials 16 (2001) 301–310.
[18] Y. Shen, R. Chen, F. Xiao, H. Sun, A. Tok, Z. Dong, Study of the cation distributions in Eu doped $Sr_2Y_8(SiO_4)_6O_2$ by X-ray diffraction and photoluminescent spectra, Journal of Solid State Chemistry 183 (2010) 3093–3099.
[19] Y. Shen, A. Tok, Z. Dong, Synthesis and crystal structure characterization of silicate apatite $Sr_2Y_8(SiO_4)_6O_2$, Journal of the American Ceramic Society 93 (2010) 1176–1182.
[20] W.J. Weber, L.M. Wang, Effect of temperature and recoil-energy spectra on irradiation-induced amorphization in $Ca_2La_8(SiO_4)_6O_2$, Nuclear Instruments and Methods in Physics Research Section B 91 (1994) 63–66.
[21] K. Fukuda, T. Asaka, R. Hamaguchi, T. Suzuki, H. Oka, A. Berghout, E. Bechade, O. Masson, I. Julien, E. Champion, P. Thomas, Oxide-ion conductivity of highly *c*-axis-oriented apatite-type lanthanum silicate polycrystal formed by reactive diffusion between La_2SiO_5 and $La_2Si_2O_7$, Chemistry of Materials 23 (2011) 5474–5483.
[22] D.W. Matson, S.K. Sharma, J.A. Philpotts, The structure of high-silica alkali-silicate glasses. A Raman spectroscopic investigation, Journal of Non-crystalline Solids 58 (1983) 323–352.
[23] Y.S. Chou, E.C. Thomsen, J.P. Choi, J.W. Stevenson, Compliant alkali silicate sealing glass for solid oxide fuel cell applications: combined stability in isothermal ageing and thermal cycling with YSZ coated ferritic stainless steels, Journal of Power Sources 197 (2012) 154–160.
[24] T. Chappex, K.L. Scrivener, The influence of aluminium on the dissolution of amorphous silica and its relation to alkali silica reaction, Cement and Concrete Research 42 (2012) 1645–1649.
[25] M.D. Dramićanin, V. Jokanović, B. Viana, E. Antic-Fidancev, M. Mitrić, Ž. Andrić, Luminescence and structural properties of Gd_2SiO_5:Eu^{3+} nanophosphors synthesized from the hydrothermal obtained silica sol, Journal of Alloys and Compounds 424 (2006) 213–217.
[26] B. Grobelna, P. Bojarski, Red emission of Eu (III) ions doped gadolinium or lanthanum tungstate entrapped in silica xerogel, Journal of Non-crystalline Solids 355 (2009) 2309–2313.
[27] G. Ju, Y. Hu, H. Wu, Z. Yang, C. Fu, Z. Mu, F. Kang, A red-emitting heavy doped phosphor $Li_6Y(BO_3)_3$:Eu^{3+} for white light-emitting diodes, Optical Materials 33 (2011) 1297–1301.
[28] M.H. Werts, R.T. Jukes, J.W. Verhoeven, The emission spectrum and the radiative lifetime of Eu^{3+} in luminescent lanthanide complexes, Physical Chemistry Chemical Physics 4 (2002) 1542–1548.
[29] X.Y. Chen, G.K. Liu, The standard and anomalous crystal-field spectra of Eu^{3+}, Journal of Solid State Chemistry 178 (2005) 419–428.
[30] D.K. Williams, B. Bihari, B.M. Tissue, J.M. McHale, Preparation and fluorescence spectroscopy of bulk monoclinic Eu^{3+}:Y_2O_3 and comparison to Eu^{3+}:Y_2O_3 nanocrystals, Journal of Physical Chemistry B 102 (1998) 916–920.
[31] S. Long, J. Hou, G. Zhang, F. Huang, Y. Zeng, High quantum efficiency red-emission tungstate based phosphor $Sr(La_{1-x}Eu_x)_2Mg_2W_2O_{12}$ for WLEDs application, Ceramics International 39 (2013) 6013–6017.
[32] B. Yang, Z. Yang, Y. Liu, F. Lu, P. Li, Y. Yang, X. Li, Synthesis and photoluminescence properties of the high-brightness Eu^{3+}-doped $Sr_3Y(PO_4)_3$ red phosphors, Ceramics International 38 (2012) 4895–4900.
[33] L.M. Wang, W.J. Weber, Transmission electron microscopy study of ion-beaminduced amorphization of $Ca_2La_8(SiO_4)_6O_2$, Philosophical Magazine 79 (1999) 237–253.
[34] P. Babu, K.H. Jang, E.S. Kim, R. Vijaya, C.K. Jayasankar, V. Lavín, H.J. Seo, Local field dependent fluorescence properties of Eu^{3+} ions in a fluorometaphosphate laser glass, Journal of Non-Crystalline Solids 357 (2011) 2139–2147.
[35] R. Ternane, G. Panczer, M.T. Cohen-Adad, C. Goutaudier, G. Boulon, N. Kbir-Ariguib, M. Trabelsi-Ayedi, Relationships between structural and luminescence properties in Eu^{3+}-doped new calcium borohydroxyapatite, Optical Materials 16 (2001) 291–300.
[36] X.H. Chuai, H.J. Zhang, F.S. Li, S.Z. Lu, J. Lin, S.B. Wang, K. Chi-Chou, Synthesis and luminescence properties of oxyapatite $NaY_9Si_6O_{26}$ doped with Eu^{3+}, Tb^{3+}, Dy^{3+} and Pb^{2+}, Journal of Alloys and Compounds 334 (2002) 211–218.
[37] S. Ferdov, R.A. Sa Ferreira, Z. Lin, Hydrothermal synthesis, structural investigation, photoluminescence features, and emission quantum yield of Eu and Eu–Gd silicates with apatite-type structure, Chemistry of Materials 18 (2006) 5958–5964.
[38] M.G. Zuev, A.M. Karpov, A.S. Shkvarin, Synthesis and spectral characteristics of $Sr_2Y_8(SiO_4)_6O_2$:Eu polycrystals, Journal of Solid State Chemistry 184 (2011) 52–58.
[39] Y. Chen, H.K. Yang, S.W. Park, B.K. Moon, B.C. Choi, J.H. Jeong, K.H. Kim, Characterization and photoluminescent enhancement of Li^+ corporation effect on $CaWO_4$:Eu^{3+} phosphor, Journal of Alloys and Compounds 511 (2012) 123–128.
[40] Y.C. Li, Y.H. Chang, B.S. Tsai, Y.C. Chen, Y.F. Lin, Luminescent properties of Eu-doped germanate apatite $Sr_2La_8(GeO_4)O_2$, Journal of Alloys and Compounds 416 (2006) 199–205.
[41] M. Buijs, A. Meyerink, G. Blasse, Energy transfer between Eu^{3+} ions in a lattice with two different crystallographic sites: Y_2O_3: Eu^{3+}, Gd_2O_3: Eu^{3+} and Eu_2O_3, Journal of Luminescence 37 (1987) 9–20.